Offline Routing and Regenerator Placement and Dimensioning for Translucent OBS Networks

Oscar Pedrola, Davide Careglio, Miroslaw Klinkowski, and Josep Solé-Pareta

***Abstract*—The deployment of translucent optical networks is considered the most promising short term solution to decrease costs and energy consumption in optical backbone networks. In fact, translucent wavelength switched optical networks (WSONs) have recently received great attention from the research community due to their technological maturity. However, the inflexibility and coarse granularity of WSONs is (re-)fostering research interest in sub-wavelength switching technologies such as optical burst switching (OBS). In OBS, however, the majority of research works neglect the impact of physical layer impairments by considering either fully transparent (i.e., with optical 3R regeneration) or opaque (i.e., with electrical 3R regeneration) networks. For this very reason, in this paper we present a translucent OBS (T-OBS) network architecture which aims at bridging the gap between the transparent and opaque solutions. In the T-OBS network the problem of routing and regenerator placement and dimensioning (RRPD) emerges. Joint RRPD is a complex problem and, in order to approach it, we propose to decompose it into the routing and RPD subproblems. As a consequence, we provide a mixed integer linear programming formulation of the routing problem and several heuristic strategies for the RPD problem. Illustrative numerical results prove the effectiveness of these methods at minimizing the number of electrical 3R regenerators deployed in the network. Considering a broad range of network topologies, we show that the proposed RPD heuristics ensure a proper quality of transmission performance whilst at the same time providing a cost-effective T-OBS network architecture.**

***Index Terms*—Optical burst switching; Physical layer impairments; Routing and regenerator placement.**

I. Introduction

Owing to the natural evolution of optical networks from traditional opaque toward transparent architectures, the consideration of physical layer impairments (PLIs) such as crosstalk, chromatic and polarization mode dispersion, noise accumulated due to amplified spontaneous emission (ASE), etc. has become unavoidable [1]. In an opaque network, the impact of PLIs can be neglected due to the fact that optical signals (carrying traffic) terminate at each node (i.e., each transmission is a point-to-point connection), and, thus, are implicitly regenerated. In contrast, in a transparent network, optical signals originated at source nodes must reach their final destination optically bypassing all intermediate nodes. This approach considerably reduces the network cost since neither optical–electrical–optical (O/E/O) conversions nor electronic processing is required at any node along the path. However, the limited transmission reach of optical signals and the lack of full all-optical regeneration devices prevent the deployment of transparent optical networks [2], at least until these limitations are overcome.

Hence, the consideration of translucent architectures [3] as a feasible intermediate step in the migration toward fully transparent optical networks has gained huge momentum. Note that, in translucent networks, regenerators[1] are only available at selected nodes, a fact which makes this architecture an ideal yet feasible candidate for bridging the gap between the transparent and opaque solutions. Indeed, due to the technological maturity of translucent wavelength switched optical network (WSON) architectures, they have already caught considerable attention from the research community (see, e.g., [4,5]).

This is not, however, the case for optical burst switching (OBS), which is a well-known approach providing sub-wavelength switching granularity [6]. So far, the research efforts on OBS have been mainly geared toward evaluating the opaque and transparent architectures. Considering either of these two network scenarios allows one to neglect the impact of PLIs, thereby notably simplifying the design and operation of OBS. Indeed, as long as realistic core node parameters (e.g., node degree and link and wavelength capacity) are considered, the optical signal degradation between two neighboring core nodes is not an issue [7]. Unfortunately, however, the high cost of O/E/O devices on the one hand, and the lack of mature optical technology able to perform fully optical 3R regeneration on the other, hamper the deployment of these architectures. Therefore, there is no way to neglect the severe impact that PLIs have on the performance of OBS networks. For this very reason, in [8], we presented a translucent OBS (T-OBS) network architecture in which core nodes switch incoming data bursts to their output ports either in an all-optical fashion or through regenerators when signal regeneration is required.

Manuscript received March 30, 2011; revised July 8, 2011; accepted July 13, 2011; published August 11, 2011 (Doc. ID 145024).

Oscar Pedrola (e-mail: opedrola@ac.upc.edu), Davide Careglio, and Josep Solé-Pareta are with the Department of Computer Architecture, Universitat Politècnica de Catalunya, Barcelona, Catalunya 08034, Spain.

Miroslaw Klinkowski is with the National Institute of Telecommunications, 51-501 Wroclaw, Poland.

Digital Object Identifier 10.1364/JOCN.3.000651

[1] If not specifically given differently, in this paper the term regenerator implicitly refers to the electrical 3R regenerator in which the regeneration of the optical signal is achieved by means of the O/E/O conversion.

1943-0620/11/090651-16/$15.00

For translucent optical networks to attract continuing interest, they should be designed in such a way that both the cost and the power consumption are minimized. Both constraints are clearly related to the number of regenerators deployed across the network and, therefore, their number must be reduced as much as possible. For this reason, the definition of algorithms either for regenerator placement (RP) [9] or for routing and regenerator placement (RRP) (see, e.g., [10,11]), if routing and wavelength assignment (RWA) constraints are added to the problem, is essential to the problem's success. These techniques are aimed at minimizing the number of regenerators deployed in a WSON by finding their optimal location. The use of RP or RRP solutions is nevertheless not viable for OBS due to its statistical multiplexing nature. Indeed, in contrast to WSONs, where there exists a one-to-one correspondence between a path and a regenerator, in OBS, regenerator resources are statistically shared (i.e., according to their timely availability) by all bursts requiring regeneration. To tackle this issue, in [8] we introduced the so-called routing and regenerator placement and dimensioning (RRPD) problem. Here it is worth stressing the novelty of our solution which incorporates the dimensioning phase that clearly distinguishes it from the RRP problem applied in WSONs. This phase is needed to ensure that only a small portion of bursts (e.g., 10^{-4}) competing for regenerator resources cannot be regenerated and thus are dropped due to their accumulated PLI. Recently in [12], and driven by the fact that the joint RRPD problem leads to a very complex model formulation, we presented a formal model to solve R+RPD, that is, we simplified RRPD by decoupling it into the routing and RPD subproblems. To this end, we provided mixed integer linear programming (MILP) formulations to solve both the routing and RPD subproblems separately. However, RPD is still complex when large problem instances are considered, and, consequently, we proposed and evaluated two straightforward RPD methods, both aimed at grouping regenerators in as few nodes as possible.

In this paper, we extend the preliminary works presented in [8] and [12] with the goal of developing heuristics able to provide a high quality trade-off between optimality and computational complexity. Specifically, we illustrate a model to capture the impact of the main PLIs which uses the optical signal to noise ratio (OSNR) as the signal quality of transmission (QoT) performance indicator. Afterward, and using such a PLI model as a constraint, we deal with RRPD by tackling the routing and RPD subproblems separately. First, we present MILP formulations aimed at minimizing congestion in network bottleneck links (a routing subproblem). Second, we develop a set of heuristic methods whose aim is to minimize the number of regenerators required to keep losses caused by PLIs under a reasonable degree of control (an RPD subproblem). The RPD heuristics are based, among others, on the ant colony optimization (ACO) [13] theory and the biased random-key genetic algorithm (BRKGA) [14]. Then, we thoroughly assess the quality of these heuristics by comparing their performance with that of the MILP optimal and heuristic formulations presented in [12] over a range of backbone network topologies. Finally, we study, by means of simulation, the performance of the proposed T-OBS network under the presented R+RPD strategies.

It is worth noting that the study herein presented follows a static/offline approach since RRPD decisions are taken during the network planning stage. The consideration of a dynamic traffic scenario, by contrast, would result in an online routing and regenerator allocation problem, an issue which is left out of the scope of this paper.

The rest of the paper is organized as follows. In Section II, we survey the previous work in the topics covered by this paper. In Section III, we give a complete description of both the proposed T-OBS network architecture and the OSNR network model we use to capture the impact of the main PLIs. In Section IV, the RRPD problem is defined. Later, Sections V and VI present, respectively, a formal model to solve the routing problem and several heuristic methods to help solve the RPD issue. All strategies proposed are exhaustively tested and evaluated in Section VII. Finally, concluding remarks are made in Section VIII.

II. Related work

Due to the fact that WSONs rely on already mature technology, the study and evaluation of translucent WSONs have recently received increasing attention from the research community (e.g., [2,3]) and a standardization activity has started in the Internet Engineering Task Force (IETF) within the Common Control and Measurement Plane (CCAMP) working group [4]. For a translucent optical network to work properly, a limited set of regenerators must be strategically deployed across the network for signal regeneration purposes [15]. This is a planning problem where a clear trade-off between network construction costs (i.e., O/E/O devices are expensive) and service provisioning performance (i.e., proper optical end-to-end QoT must be ensured) exists. Therefore, both the RWA and the RP issues must be carefully engineered. However, both the RWA and the RP problems as well as the joint RRP problem are known to be N-complete [9], and, hence, heuristic approaches are generally employed [16]. For a recent compelling work on the joint RWA and regenerator allocation problem in translucent WSONs we refer the reader to [17] and to its references. So far, the research on OBS has been mainly focused on both the opaque and the transparent network architectures, and as a result of this, the vast majority of the research works consider that either the physical layer is ideal (i.e., without impairments) or signal regenerators are available at every channel (i.e., OBS is either fully transparent or fully opaque). Recently, however, owing to the increasing interest in assessing the effect of the PLIs in the optical network field, we find a few interesting works that involve the PLI constraint in the evaluation of the OBS network performance. For example, in [18] the authors deal with a burst scheduling method which incorporates the impairments constraint, and in [19], several impairment-aware algorithms to provide manycasting services in OBS networks are proposed. However, the most interesting work regarding PLIs in OBS networks can be found in [7], and its complementary study [20]. In both papers, the authors present an extensive analysis and evaluation of the design and maximum size and throughput of OBS core nodes. To this end, the authors consider the effects of a range of PLIs such as amplifier noise, crosstalk of WDM channels, gain saturation and dynamics. Nonetheless, the authors focus

on an opaque OBS network where all nodes are equipped with regenerators, which are also responsible for performing wavelength conversion.

III. Translucent OBS Network Model

In this section, we provide extensive details on the proposed translucent OBS network model. First, we specify an all-optical OBS node architecture which incorporates a limited number of shared electrical regenerators. Second, we present the analytic model that we consider for the calculation of the OSNR level. Finally, a power budget and noise analysis of the characteristic signal path between two adjacent OBS nodes is provided.

In general, in an OBS network there are two types of nodes, namely, edge and core nodes. In OBS, the transport of client data, which are aggregated from different sources (e.g., IP packet traffic, Ethernet), is based on the following principles. Edge nodes are in charge of both assembling client input packets into outgoing bursts and disassembling incoming bursts. For each outgoing burst, edge nodes emit a separate burst control packet (BCP) in advance, to reserve resources (i.e., bandwidth on a desired output channel) along the way from the ingress node to an egress node. Core nodes and their corresponding control units are responsible for reading and processing BCPs and for switching individual bursts accordingly. In OBS, core nodes are generally assumed to be wavelength conversion capable.

A. Node Architecture

The node architecture here presented is based on the model proposed in [7], which initially assumes an opaque operation. To be precise, the authors present two semiconductor optical amplifier (SOA)-based node architectures for OBS networks, namely, broadcast-and-select (BAS) and tune-and-select (TAS). Both architectures rely on the SOA technology and on wavelength converters performing electrical 3R regeneration as their fundamental switching modules. SOAs acting as switching elements (SW-SOA) bring some interesting advantages such as high on/off ratios and high loss compensation characteristics. Despite this, however, SOA technology also entails some non-desirable effects such as power consumption, noise and non-linearity that must be taken into account during the node design process. Among these architectures, the authors conclude that TAS is more appropriate for OBS networks because BAS displays some major drawbacks (e.g., high power requirements and large interchannel crosstalk) inherent to its architecture.

In this paper, we modify the aforementioned opaque TAS OBS core node architecture by replacing each in-line electrical wavelength converter with a block consisting of a tunable laser and a wavelength conversion-type SOA (WC-SOA) device. Hence, this modified TAS node architecture (depicted in Fig. 1) is able to perform an all-optical switching operation. The node consists of N input/output fibers with M channels each and a limited number R of regenerators available. After the signal is amplified by the erbium-doped fiber amplifier (EDFA) pre-amplifier at each node input port, it is demultiplexed and

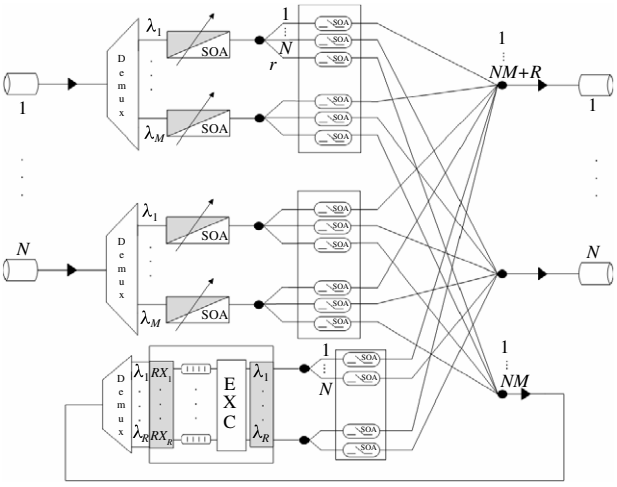

Fig. 1. T-OBS node architecture [8].

passes through a fixed-input and variable-output WC-SOA. Then, the signal is split into $N+1$ branches, one per fiber plus an extra branch that allows access to the regenerator pool, which consists of a set of R fixed receivers, an electrical buffering stage and a set of R lasers emitting in predefined wavelengths (i.e., $\lambda_1,\ldots,\lambda_R$). The signal is then transported to the output ports of the node following the decisions of the OBS node controller by turning the SW-SOAs either ON or OFF. After the combiner stage, an EDFA booster amplifier provides the signal with enough power to cope with the losses of the first fiber span. Note also that, in this case, the combiners behind the SW-SOA port merge $NM+R$ signals at each output port as a consequence of the presence of the regenerator pool.

It is worth mentioning that since the output of the WC-SOA is handled by the OBS node controller, all wavelengths from all input ports have the same privileges when requesting a regenerator, and, thus, fairness in the access to the regenerator pool is provided by this architecture.

We also point out that our offline planning approach requires that a burst, whenever sent on a path, will be regenerated only at the nodes that are specified as regenerative sites for this particular path. To signalize these sites, source nodes include in the BCPs the information regarding the set of nodes where their corresponding data burst has to be regenerated. We assume that BCPs do not suffer from non-compliant OSNR levels since, for processing purposes, they always undergo an O/E/O conversion (i.e., are regenerated) at each node.

In the following subsections, we evaluate the performance of the proposed node architecture by means of an OSNR model.

B. OSNR Model

In this OSNR model, the impact of PLIs is captured by considering the power of both the signal and the noise, which are affected by different gains and losses along the path, at the destination node. This model considers the ASE noise introduced by both the EDFA and SOA amplifiers as well as the splitting and attenuation losses as the significant

signal impairment factors [21]. In the literature, OSNR is generally defined as the ratio between the signal channel power and the power of the ASE noise in a specified bandwidth (e.g., 0.1 nm is usually taken by convention). For instance, for a transparent WSON an OSNR model is proposed and evaluated in [22], and it is experimentally validated in [21]. Thus, all bursts arriving at the destination node with an accumulated OSNR value lower than a predefined quality threshold (T_{osnr}) cannot be read correctly, and, thus, are discarded. Although ASE noise is commonly considered as the most severe impairment limiting the reach and capacity of optical systems, in OBS networks, non-linear impairments arising both from its inherent ON–OFF switching nature and from dynamic power fluctuations generated by gain changes in amplifiers may strongly impact system performance. Indeed, these fast ON–OFF transitions cause sudden power variations in every single channel, resulting in a variety of non-linear phenomena degrading the optical signal, for instance, cross-phase modulation (XPM)-induced crosstalk in a burst caused by neighboring bursts co-propagating simultaneously over several common links. To take these effects into account, we use an OSNR penalty on the OSNR threshold as defined in [21]:

$$T_{\text{osnr}} = T_{\text{osnr-min}} + T_{\text{osnr-pen}}, \tag{1}$$

where $T_{\text{osnr-min}}$ represents the OSNR tolerance of the receiver and $T_{\text{osnr-pen}}$ accounts for the OSNR penalties due to maximum tolerable polarization mode dispersion (PMD), residual chromatic dispersion (CD) and all the other non-linearities. We assume that $T_{\text{osnr-pen}}$ is configured by the network operator according to the transmitted signal bitrate, modulation format, etc. [21]. Note that in systems where non-linear impairments are dominant either larger values of $T_{\text{osnr-pen}}$ should be set up (with a possible impact on the network performance) or more accurate and computationally efficient analytical models to capture dynamic PLIs have to be developed. To quantify the OSNR degradation along the optical path, we define the optical path OSNR (P_{osnr}) by adapting the model described in [23]. Specifically, the OSNR consists of two main components, namely, the link and node OSNRs that we denote as L_{osnr} and N_{osnr}, respectively. Since a link is composed of several amplifier spans, each ending with an in-line EDFA amplifier, the longer the path the higher the impact of the ASE noise in the OSNR received. Similarly, to minimize the ASE effect caused by the internal node amplifiers, gain values should be designed such that each node presents an OSNR level as high as possible. We can compute P_{osnr} for an optical end-to-end path traversing k links by using the following equation [23]:

$$P_{\text{osnr}} = 1/\left(\sum_{i=1}^{k} \frac{1}{L^i_{\text{osnr}}} + \sum_{i=1}^{k} \frac{1}{N^i_{\text{osnr}}}\right), \tag{2}$$

where for a link consisting of r amplifier spans, L^i_{osnr} is defined as follows:

$$L^i_{\text{osnr}} = 1/\left(\sum_{j=1}^{r} \frac{1}{AS^j_{\text{osnr}}}\right), \tag{3}$$

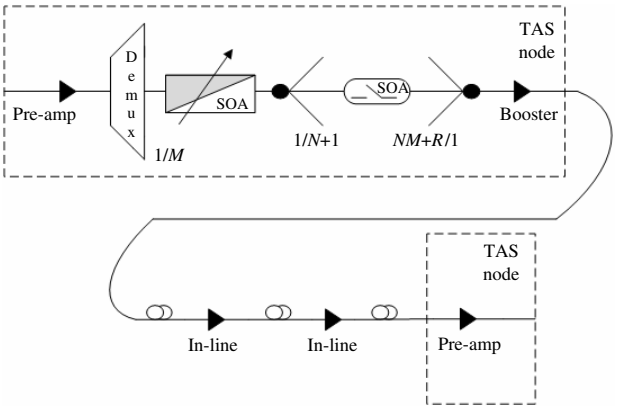

Fig. 2. Signal path between two TAS OBS core nodes.

where AS^j_{osnr} is the amplifier span OSNR, which can be calculated as

$$AS^j_{\text{osnr}}[\text{dB}] = P_j[\text{dBm}] - QN[\text{dBm}] - F_j[\text{dB}] - G_j[\text{dB}], \tag{4}$$

where P_j, QN, F_j and G_j, correspond to the output power after the j^{th} amplifier span, the quantum noise, the noise figure and the gain of the j^{th} amplifier (i.e., either EDFA in-line or pre-amplifier), respectively. The expression that we use to compute N_{osnr} is equal to the one that we have defined for AS_{osnr}; however, due to the presence of several components (e.g., amplifiers, splitters and combiners) in our translucent node, both an equivalent noise and a gain figure, namely, F_{eq} and G_{eq}, respectively, have to be derived.

In the next subsection, we provide specific values for all these parameters by considering performance values obtained from datasheets of commercially available or lab trial devices (see, e.g., [24–26]).

C. Power Budget and Noise Analysis

We consider the power and noise constraints together in order to evaluate the OSNR of a signal that follows the characteristic path between two TAS neighboring nodes depicted in Fig. 2. Component specifications are provided in Table I and the power constraints for this analysis are the output power of the node (i.e., output of the EDFA booster amplifier) set to 0 dBm/channel and its input power (i.e., input of the EDFA pre-amplifier) set by link losses to −16 dBm/channel.

From Eq. (4) and bearing in mind that the objective is to have an N_{osnr} as high as possible, it can be inferred that both F_{eq} and G_{eq} must be designed so that their resultant values are minimized. For this particular case, the equivalent noise and gain figures of the TAS node are obtained as follows:

$$F_{\text{eq}} = F_{\text{wc-soa}} + \frac{MF_{\text{sw-soa}} - 1}{\frac{G_{\text{wc-soa}}}{L_{\text{splitter}}}} + \frac{F_{\text{edfa-booster}} - 1}{\frac{G_{\text{wc-soa}}G_{\text{sw-soa}}}{L_{\text{splitter}}L_{\text{combiner}}}}, \tag{5}$$

$$G_{\text{eq}} = \frac{G_{\text{wc-soa}}G_{\text{sw-soa}}G_{\text{edfa-booster}}}{L_{\text{splitter}}L_{\text{combiner}}}. \tag{6}$$

TABLE I
PARAMETER VALUES CONSIDERED

Channels (M)	32	
Span length	65 km	
Fiber attenuation	0.2 dB/km + 3 dB (cable margin)	
Quantum noise	−58 dBm	
EDFA (pre-amp)	Noise figure Max. gain Max. output power Min. input power	5.5 dB 20 dB 13 dBm −30 dBm
EDFA (booster)	Noise figure Max. gain Max. output power Min. input power	5.5 dB 15 dB 18 dBm −15 dBm
EDFA (in-line)	Noise figure Max. gain Max. output power Min. input power	5.5 dB 25 dB 18 dBm −25 dBm
WC-SOA	Noise figure Max. gain Max. output power Min. input power	9 dB 16 dB 5 dBm −25 dBm
SW-SOA	Noise figure Max. gain Max. output power Rise–fall time	10 dB 10 dB 3 dBm 500 ps
WDM demux	Insertion loss ($M = 32$)	(≈5.5) dB
Splitter	Insertion loss	(0.5–1) dB
Combiner	Insertion loss	(1.5–2) dB

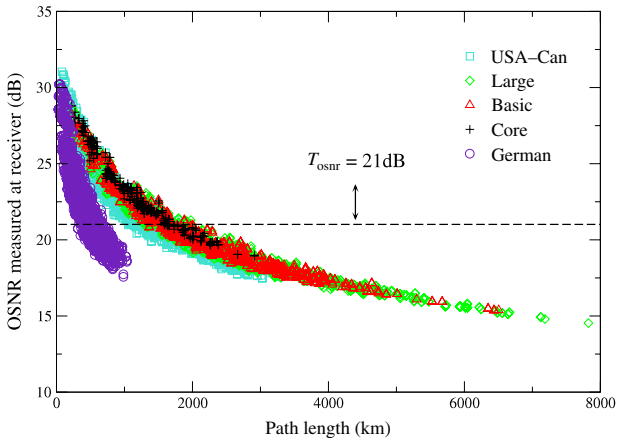

Fig. 3. (Color online) OSNR evaluation for some European and American network end-to-end optical paths.

The most critical point is the combiner where, in the worst case, the ASE noise power from M SW-SOAs is merged. Both the pre-amplifier and booster EDFAs and the WC-SOA and SW-SOA have to be used to compensate the internal losses. Their gain values must be carefully designed so that both equivalent figures are minimized and the power constraints are respected. In order to minimize F_{eq}, it can be deduced from Eq. (5) that, as long as the saturation output power is not reached, it is better to set the gain on the WC-SOA. In this way, the impact of the M ASE powers is reduced. The EDFAs' pre-amplifier and booster and SW-SOA gains, by contrast, are kept as low as allowed by the system power requirements. The exact setup for each component depends on the number of input/output ports of each particular node, which eventually define the splitting losses that are to be covered by G_{eq}.

In Fig. 3, we show the result of the application of the OSNR model presented considering the optical end-to-end paths of the pan-European core transport network in three different topology configurations (large, basic and core), a German backbone topology and an American backbone network (USA–Can). See Appendix A for the simulation details. All network paths are computed making use of the routing algorithm presented in Section V. One can observe that, with the exception of the German topology, the length, and thus the number of amplifier spans, have a strong impact on the received OSNR. In the German network, which is characterized by much shorter links and by a high number of nodes (see Appendix A), by contrast, it is the number of intermediate nodes that has the greater impact on the OSNR figure. The next Section is devoted to presenting a formal model to solve the RRPD problem considering both the T-OBS network architecture and the OSNR network model described.

IV. RRPD PROBLEM

A. Problem Definition and Solution Approach

In this section, we present our approach to the offline RRPD planning problem in T-OBS networks and detail the assumptions we make in order to solve it. The objective of our offline RRPD problem is to find, for a given set of traffic demands, 1) the set of explicit paths to be used to route bursts through the network, 2) the placement of regenerator sites in selected nodes on those paths having unacceptable OSNR at the receiving end and 3) the number of such regenerators in each node in order to guarantee a given target burst loss probability.

The complexity of the RRPD problem is high due to the joint consideration of the routing, regeneration placement and regenerator dimensioning problems. In order to reduce this complexity, in our approach we decouple the routing problem from the RPD problem. The main reason supporting this decision is the fact that in OBS networks routing must be carefully engineered since the main source of performance degradation is the contention between bursts that arise due to both the lack of optical buffering and the generally considered one-way resource reservation scheme. Hence, given a set of traffic demands, we first find a proper routing that minimizes burst losses due to congestion in bottleneck network links. Afterward, this routing solution is used as input information to solve the RPD problem which eventually aims at minimizing the number of regenerators deployed in the network.

Accordingly, in Section V we present an optimal routing algorithm based on an MILP formulation. Later, in Section VI, we propose and detail four different heuristic methods to solve the RPD problem.

B. General Notation

We use $\mathcal{G}=(\mathcal{V},\mathcal{E})$ to denote the graph of the T-OBS network; the set of nodes is denoted as $\mathcal{V}$, and the set of unidirectional links is denoted as $\mathcal{E}$. Let $\mathcal{P}$ denote the set of predefined candidate paths between source s and termination t nodes, $s,t\in\mathcal{V}$ and $s\neq t$. Each path $p\in\mathcal{P}$ is identified with a subset of network links, that is, $p\subseteq\mathcal{E}$. Adequately, subset $\mathcal{P}_e\subseteq\mathcal{P}$ denotes all paths that go through link e. Let s_p and t_p denote the source and termination nodes of p. Let $\mathcal{N}_p$ be the set of all nodes constituting path p and let $\mathcal{V}_p$ denote the set of intermediate nodes on path p such that $\mathcal{V}_p=\mathcal{N}_p\setminus\{s_p,t_p\}$. Let $\mathcal{D}$ denote the set of demands, where each demand corresponds to a pair of source–termination nodes. Let $h_d=\lambda_d/\mu$ denote the average offered burst traffic load for demand $d\in\mathcal{D}$, where λ_d is the average burst arrival rate and μ is the average burst service rate. Finally, let $\mathcal{P}_d\subseteq\mathcal{P}$ denote the set of candidate paths supporting demand d, where $\mathcal{P}=\bigcup_{d\in D}\mathcal{P}_d$. Each subset $\mathcal{P}_d$ comprises a (small) number of paths, for example, k shortest paths.

V. Routing Algorithm

For the routing algorithm, we consider a modified MILP formulation of the linear programming (LP) algorithm proposed in [27]. To be precise, the presented algorithm consists in solving, sequentially, two MILP models in order to find a solution to the routing problem. The objective is to distribute the traffic over a set of candidate paths so that congestion in network bottleneck links is reduced. The network applies source routing, and hence the source node determines the path that a burst must follow in the network.

Let variable y represent the average traffic load on the bottleneck link. The first MILP formulation aims at minimizing the load on such a particular link:

$$\textit{minimize}\quad y \tag{RMILP1}$$

subject to

$$\sum_{p\in\mathcal{P}_e} x_p h_d - y \le 0,\quad \forall e\in\mathcal{E}, \tag{7a}$$

$$\sum_{p\in\mathcal{P}_d} x_p = 1,\quad \forall d\in\mathcal{D}, \tag{7b}$$

$$x_p\in\{0,1\},\quad \forall p\in\mathcal{P}, \tag{7c}$$

where the selection of path p from set $\mathcal{P}_d$ is performed according to a decision variable x_p, which says that a burst flow is routed over path p iff $x_p=1$. Moreover, there is only one path $p\in\mathcal{P}_d$ such that $x_p=1$. The traffic load ρ_p of path $p\in\mathcal{P}$ is hence $\rho_p=x_p h_d$.

Despite minimizing the average traffic load on the bottleneck link, many solutions to this problem may exist and most of them exploit unnecessary resources in the network (i.e., solutions that select longer paths). Therefore, the next MILP is solved in order to obtain, among the solutions of Eq. (RMILP1), the one that entails the minimum increase of the average traffic load offered to the remaining network links. For this purpose, let us denote y^* as an optimal solution of Eq. (RMILP1), then we solve the following problem:

$$\textit{minimize}\sum e\in\mathcal{E}\sum_{p\in\mathcal{P}_e} x_p h_d \tag{RMILP2}$$

subject to

$$\sum_{p\in\mathcal{P}_e} x_p h_d \le y^*,\quad \forall e\in\mathcal{E} \tag{8}$$

and subject to the routing constraints given by Eqs. (7b) and (7c). Note that, in constraint (8), we ensure that the maximum average traffic load on the bottleneck link is bounded by the solution of Eq. (RMILP1).

These MILP models, if sequentially solved, determine the path p that will be in charge of carrying the traffic for each demand d. Hence, only one path $p_d\in\mathcal{P}_d$ is selected as the valid path to be followed by all bursts belonging to demand d. Thus, we can now denote $\mathcal{Q}$ as the set of valid paths, $\mathcal{Q}=\{p_d,d\in\mathcal{D}\}$.

VI. Heuristic RPD Algorithms

The objective of the RPD problem is to determine both the sites where regenerators must be placed and the amount of such regenerators in every selected site so that a successful regeneration for a given percentage of bursts is guaranteed. This implies that only a given (small enough) ratio of bursts cannot be regenerated due the fair competitive (statistical multiplexing) access to the regenerators and consequently are lost.

Let $\mathcal{P}^o\subseteq\mathcal{Q}$ denote the subset of paths for which the OSNR level at receiver t is non-compliant with the QoT requirements, and, thus, paths $p\in\mathcal{P}^o$ that require regeneration at some node $v\in\mathcal{V}_p$. For each path p, there may exist many different options on how to build an end-to-end OSNR compliant path, composed by its transparent segments, since the node or group of nodes where the regeneration can be performed is generally not a unique solution. Thus, let $\mathcal{S}_p=\{s_1,\ldots,s_{|\mathcal{S}_p|}\}$ denote the set of different options to establish an OSNR compliant path for each path $p\in\mathcal{P}^o$, where $s_i\subseteq\mathcal{V}$, $i=1\ldots|\mathcal{S}_p|$ and $|\mathcal{S}_p|$ depends on the length of the transparent segments in path p. To obtain $\mathcal{S}_p, p\in\mathcal{P}^o$, a precomputation phase is executed to obtain all possible regeneration options using the OSNR model described in Subsection III.B as the QoT constraint. To illustrate this concept by means of an example, let us consider an OSNR non-compliant path p^o between source node 1 and destination node 5 crossing intermediate nodes 2, 3 and 4. In p^o, the precomputation phase may find three different regenerator allocation options (e.g., $s_1=\{3\}$, $s_2=\{2,4\}$ and $s_3=\{2,3,4\}$), all of them ensuring that the OSNR level at every node along p^o is above the system T_{osnr} threshold.

We assume that for each path $p\in\mathcal{P}^o$, the selection of the regeneration option s from set $\mathcal{S}_p$ is performed according to a decision variable z_{ps} such that the following constraints are fulfilled:

$$\sum_{s\in S_p} z_{ps} = 1,\quad \forall p\in\mathcal{P}^o, \tag{9a}$$

$$z_{ps}\in\{0,1\},\quad \forall s\in\mathcal{S}_p,\forall p\in\mathcal{P}^o. \tag{9b}$$

The goal of the RPD algorithm is hence to select for each path $p \in \mathscr{P}^o$ the regenerative option $s \in \mathscr{S}_p$ which minimizes the total number of regenerators deployed in the network. In the following subsections, we propose four different offline heuristic RPD algorithms. For the sake of clarity, we consider an objective function denoted by $g(\cdot)$ which accounts for the calculation of the number of regenerators required. This is achieved by calling the dimensioning function whose pseudo-code is shown in Procedure 5 in Subsection VI.E. Although this procedure may be called several times within the RPD heuristics next presented, the solutions of Procedure 5 are precomputed only once at the very beginning of the algorithm and stored in an ordered array, thereby substantially reducing the time complexity (see details in Subsection VI.E). Hence, we do not include this factor in the complexity analysis of the heuristic RPD algorithms presented below.

A. KL Local Search (KLS) Algorithm

The KLS algorithm is a heuristic algorithm which is based on the KL local search technique [28]. In this algorithm, we assume a neighboring solution is achieved by means of a flip operation which consists of a permutation of the regeneration sites for a specific set of demands. The pseudo-code of the KLS algorithm is shown in Procedure 1. Let $\mathscr{R}_z$ be the set of all regeneration vectors that define for each path $p \in \mathscr{P}^o$ the node or set of nodes where the regeneration is performed, that is, $\mathscr{R}_z = \bigcup_{p\in\mathscr{P}^o} \mathbf{z}_p$, where $\mathbf{z}_p = (z_{p1},\ldots,z_{p|\mathscr{S}_p|})$. Then, let $\mathscr{R}_o$ be an initial (randomly selected) solution to the problem where constraints (9a) and (9b) are met for each $\mathbf{z}_p, p \in \mathscr{P}^o$.

Similarly, let $\mathscr{R}_{tb}$, $\mathscr{R}_i$ and $\mathscr{R}_b$ denote, respectively, the global best solution obtained so far, the best solution of a whole iteration and one of the solutions of the iteration in progress. Moreover, let $\Omega_{\mathscr{R}}$ be the set of valid solutions obtained once the loop between lines 5–13 in Procedure 1 is completed.

Between lines 5 and 13, starting from solution $\mathscr{R}_b$, we iteratively take, for each $p \in \mathscr{P}^o$, vector $\mathbf{z}_p \in \mathscr{R}_b$, and then we set it to $\mathbf{z}_p^*$, which is the solution for vector $\mathbf{z}_p$ that minimizes the number of regenerators to be deployed taking into account the current solutions for all other paths, that is, solutions in the current $\mathscr{R}_b$. Once a choice is made for p, then it remains fixed until the loop is initiated again.

It is also worth noticing that in line 12, an update of the current solution is performed even if it entails worsening $\mathscr{R}_b$. Procedure 1 does this in order to increase the probabilities of escaping from the local optima and in the hope that some neighboring solution generated during an iteration will turn out better than the current global best solution $\mathscr{R}_{tb}$.

To evaluate the complexity of this algorithm let us first define δ as the number of nodes constituting the largest possible path contained in $\mathscr{P}^o$, that is,

$$\delta = \max\{|\mathscr{N}_p| : p \in \mathscr{P}^o\}. \tag{10}$$

Thus, an upper bound on the maximum number of regeneration options (i.e., the maximum size for set $\mathscr{S}_p$) for a path $p \in \mathscr{P}^o$ can be derived as

$$\Theta = 2^{(\delta-2)} - 1. \tag{11}$$

Procedure 1 KLS Heuristic

INPUT: $\mathscr{P}^o, \mathscr{R}_o, \Omega_{\mathscr{R}} \leftarrow \emptyset$
OUTPUT: $g(\mathscr{R})$

1: $\mathscr{R}_{tb} \leftarrow \mathscr{R}_o$
2: $\Omega_{\mathscr{R}} \leftarrow \Omega_{\mathscr{R}} \cup \{\mathscr{R}_o\}$
3: $\mathscr{R}_b \leftarrow \mathscr{R}_o$
4: **repeat**
5: **for all** path $p \in \mathscr{P}^o$ **do**
6: $\mathscr{P}_x \leftarrow \mathscr{P}_o \backslash \{p\}$
7: Take $\mathbf{z}_p$ from $\mathscr{R}_b$
8: Determine $\mathbf{z}_p^*$ which minimizes $g(\cdot)$ considering, for all path $p \in \mathscr{P}_x$, the option $\mathbf{z}_p$ selected in $\mathscr{R}_b$
9: Let $\mathscr{R}_p$ be a new solution
10: $\mathscr{R}_p \leftarrow \mathscr{R}_b \cup \{\mathbf{z}_p^*\} \backslash \{\mathbf{z}_p\}$
11: $\Omega_{\mathscr{R}} \leftarrow \Omega_{\mathscr{R}} \cup \{\mathscr{R}_p\}$
12: $\mathscr{R}_b \leftarrow \mathscr{R}_p$
13: **end for**
14: Take $\mathscr{R}_i$ from $\Omega_{\mathscr{R}}$ which minimizes $g(\cdot)$
15: $\mathscr{R}_b \leftarrow \mathscr{R}_i$
16: $\Omega_{\mathscr{R}} \leftarrow \mathscr{R}_b$
17: **if** $g(\mathscr{R}_{tb}) > g(\mathscr{R}_i)$ **then**
18: $\mathscr{R}_{tb} \leftarrow \mathscr{R}_i$
19: **end if**
20: **until** $r_{tb} \le r_i$
21: $\mathscr{R} \leftarrow \mathscr{R}_{tb}$

Then, the complexity of Procedure 1 is given by

$$O(M \cdot |\mathscr{E}| \cdot |\mathscr{P}^o| \cdot \Theta), \tag{12}$$

where $M|\mathscr{E}|$ (the number of regenerators required in an opaque OBS network) defines an upper bound on the number of iterations at the worst case improvement (i.e., one per iteration) of the cost function. $|\mathscr{P}^o|$ accounts for the number of iterations in the *for all* loop in Procedure 1 and the last term represents the maximum number of regeneration options (Θ).

B. Regenerator Grouping (RG) Algorithm

The RG method (LCR in [12]) aims at selecting those regenerator sites which lead to solutions having the smallest possible number of nodes equipped with regenerators. The idea is that, since the access to the regenerators is subject to statistical multiplexing, grouping regenerators in few sites instead of spreading them throughout the network (thus having few regenerators in many sites) may increase its effectiveness.

In this particular algorithm, in contrast to the others, we do not make use of the precomputed set of regeneration options $\mathscr{S}_p, p \in \mathscr{P}^o$, but instead the OSNR level of each candidate transparent segment is evaluated (see lines 13 and 19 in Procedure 2). Hence, let $\mathscr{K}_p$ denote the node or set of nodes where the regeneration is performed for path p. Let $\mathscr{K} = \bigcup_{p\in\mathscr{P}^o} \mathscr{K}_p$ be the set of all nodes where the regenerators have to be installed for all paths $p \in \mathscr{P}^o$. Let Ω_p be the set of subpaths of p to be processed. Then, Procedure 2 is executed.

Procedure 2 iteratively processes each path $p \in \mathscr{P}^o$ with the aim of ensuring that the OSNR signal level meets the predefined T_{osnr} threshold at each node $v \in \mathscr{N}_p$. To

Procedure 2 RG Heuristic

INPUT: $\mathscr{P}^o$

OUTPUT: $g(\mathscr{R})$

1: $\mathscr{K} \leftarrow \emptyset, \Omega_p \leftarrow \emptyset$
2: **for all** path $p \in \mathscr{P}^o$ **do**
3: $\quad \Omega_p \leftarrow \Omega_p \cup \{p_d\}$
4: $\quad \mathscr{K}_p \leftarrow \emptyset$
5: $\quad \mathscr{T}_p \leftarrow \mathscr{K} \cap \{\mathscr{V}_p\}$
6: $\quad$ **if** $\mathscr{T}_p \neq \emptyset$ **then**
7: $\quad\quad$ Select node $v \in \mathscr{T}_p$ which is closer to the middle of the path (with respect to the number of hops)
8: $\quad\quad \mathscr{K}_p \leftarrow \mathscr{K}_p \cup \{v\}$
9: $\quad\quad \Omega_p \leftarrow \Omega_p \cup \{p_{s-v}, p_{v-t}\} \backslash \{p\}$
10: $\quad$ **end if**
11: $\quad$ **while** $\Omega_p \neq \emptyset$ **do**
12: $\quad\quad$ Take the first subpath q from Ω_p
13: $\quad\quad$ **if** q meets OSNR **then**
14: $\quad\quad\quad \Omega_p \leftarrow \Omega_p \backslash \{q\}$
15: $\quad\quad$ **else**
16: $\quad\quad\quad$ **repeat**
17: $\quad\quad\quad\quad$ Let q^* be a clone of q
18: $\quad\quad\quad\quad$ Remove the last link (and node) from q^*
19: $\quad\quad\quad$ **until** q^* meets OSNR
20: $\quad\quad\quad$ Consider t_{q^*} as the regenerative node,
21: $\quad\quad\quad \mathscr{K}_p \leftarrow \mathscr{K}_p \cup \{t_{q^*}\}$
22: $\quad\quad\quad \Omega_p \leftarrow \Omega_p \cup \{q \backslash q^*\}$
23: $\quad\quad$ **end if**
24: $\quad$ **end while**
25: $\quad \mathscr{K} \leftarrow \mathscr{K} \cup \{\mathscr{K}_p\}$
26: **end for**
27: Generate $\mathscr{R}$ from $\mathscr{K}$ and compute $g(\mathscr{R})$

provide a regenerator grouping-like behavior, in lines 5–10, the algorithm searches among all the previously processed paths if there are nodes $v \in \mathscr{V}_p$ with regenerators already installed, and, if so, it takes the node $v \in \mathscr{V}_p$ that is nearest to the middle of the path (with respect to the number of hops) and selects it as the first regeneration point for path p. Hence, two new subpaths are added to Ω_p. Between line 11 and 24, the algorithm performs a loop that adds regeneration sites to path p until Ω_p becomes an empty set. Once Procedure 2 finishes, the set of nodes $\mathscr{K}$ where the regeneration has to be performed is obtained. Note that in line 27, set $\mathscr{K}$ is mapped into set $\mathscr{R}$ so that we can apply the objective function $g(\mathscr{R})$ (Procedure 5 in Subsection VI.E).

In this case, the complexity of the algorithm is given by

$$O\left(\left|\mathscr{P}^o\right|\left(\frac{(\delta-1)(\delta-2)}{2}\right)\right), \tag{13}$$

where the second term is the upper bound on the maximum possible number of iterations required to create a feasible path, that is, when a regenerator is required at every node $v \in \mathscr{V}_p, p \in \mathscr{P}^o$. Such an operation is performed once per path $p \in \mathscr{P}^o$, and, hence, $\left|\mathscr{P}^o\right|$. Note that $\delta \geq 3$ for all paths $p \in \mathscr{P}^o$, since all paths with two nodes (just source and destination) are feasible.

C. ACO Algorithm

In this section, we propose the application of the ACO [29] methodology to solve the RPD problem. ACO was introduced in the early 1990s as a nature-inspired meta-heuristic for solving hard combinatorial optimization problems. In the field of optical networks, ACO algorithms have been used, for example, to solve the problem of RWA (see, e.g., [30–32]). ACO methods try to mimic the behavior of real ants in their task of foraging for food. Initially, an ant explores the area surrounding its nest, and when a food source is found, it evaluates the quantity and quality of its finding. Based on this measurement, the ant on its way back to the nest will deposit more or less quantity of a chemical pheromone, thereby creating a so-called pheromone trail which will subsequently help other ants to find the best possible food source. If these other ants also find food, they will reinforce the same trail by depositing more pheromone. However, if the quantity or quality of the food found decreases, the pheromone trails will tend to evaporate over time, thereby reducing the trail attractiveness.

In our problem, for each path $p \in \mathscr{P}^o = \{p_1, \ldots, p_{|\mathscr{P}^o|}\}$, we have a set of possible regeneration options $\mathscr{S}_p = \{s_1, \ldots, s_{|\mathscr{S}_p|}\}$. Let us define a variable instantiation as the assignment of a regeneration option $s_j \in \mathscr{S}_p$ to a path $p_i \in \mathscr{P}^o$, that is, $p_i = s_j$. Once an assignment for each path is performed, a feasible solution for the RPD problem is obtained. Note that we are dealing with an unconstrained problem, and, thus, each path can take any $s \in \mathscr{S}_p$ independently of the decision taken by other paths. Finally, let us also call the combination of a path p_i with a regeneration option s_j a solution component which we denote by c_i^j. Hence, we define the set of possible solution components for path p_i as $\mathscr{C}_i$. Note that $|\mathscr{C}_i| = |\mathscr{S}_{p_i}|$.

1) Pheromone Model: The pheromone model consists of a pheromone trail parameter $\mathscr{T}_i^j$ for each solution component c_i^j as proposed in [29]. This pheromone trail parameter provides the pheromone value (τ_i^j), and much as in our case τ_i^j is a function of the algorithm iteration (i.e., $\tau_i^j = \tau_i^j(t)$); this dependence will, however, be made explicit only when necessary. Eventually, we denote the whole set of pheromone trail parameters by $\mathscr{T}$. Given the fact that our interest lies in minimizing the number of regenerators and that this is better achieved if they are aggregated in as few nodes as possible, we consider that the pheromone value τ_i^j for solution component c_i^j depends exclusively on the quantity of pheromone deposited on each regeneration node $v \in s_j$ (recall that s_j consists of the set of nodes where the regeneration for path p_i is performed). Hence, we assume that each node $v \in \mathscr{V}$ has an amount of deposited pheromone equal to φ_v. Note that φ_v is like τ_i^j dependent on the algorithm iteration. Thus, the pheromone value for solution component c_i^j can be obtained as follows:

$$\tau_i^j = \sum_{v \in s_j} \varphi_v. \tag{14}$$

Besides, we consider for each solution component c_i^j a desirability factor (i.e., *heuristic information*) denoted by $\eta(c_i^j)$,

which provides a bias toward regeneration options with fewer regeneration nodes. In this case, the desirability factor is obtained as follows:

$$\eta(c_i^j) = \frac{1}{\sum_{v \in s_j} \sigma}, \tag{15}$$

where σ is a user-predefined constant parameter.

The pseudo-code of our ACO RPD algorithm is shown in Procedure 3. First, pheromone values for all nodes are initialized to a constant predefined parameter, that is, $\varphi_v = k, v \in \mathcal{V}$. Then, over a number of global iterations, a number of ants are generated to construct, independently, a solution to the problem by selecting, for each path $p \in \mathscr{P}^o$, a solution component according to a state transition rule. Hence, each ant performs the complete set of variable instantiations. Since the order in which paths are processed does have impact on the goodness of the solution, each ant has a different, randomly generated order for processing the paths in $\mathscr{P}^o$. In our ACO heuristic, we rely on two different pheromone updates, namely, a local and a global update. Whilst the former tries to bias the ant toward regeneration options which contain nodes with its own pheromone (i.e., due to previously processed paths), the latter aims at keeping track of high quality solutions by depositing more pheromone on nodes belonging to those solutions so that subsequent ants can more easily find the best trails. The state transition rule and both types of pheromone updates are next described. It is worth mentioning that some of the mathematical expressions here presented are borrowed from [29] and [32].

2) State Transition Rule: This rule is responsible for selecting the next solution component (regeneration option) in the ant regenerator allocation process (see line 10 in Procedure 3). To be precise, the transition is based on a pseudo-random-proportional rule aimed at balancing the exploration and exploitation abilities of the algorithm. Assuming the ordered set of paths to be processed, $\Lambda = \{p_1, \ldots, p_{|\mathscr{P}^o|}\}$ (see Procedure 3), the selection of the solution component c_i^j for path p_i is made according to the following rule:

$$c_i^j = \begin{Bmatrix} \max_{c_i^j \in \mathscr{C}_i} \{\tau_i^j [\eta(c_i^j)]^\beta\} & \text{if } r \le r_0 \\ Q & \text{if } r > r_0 \end{Bmatrix}, \tag{16}$$

where $r \sim U(0,1)$, and $r_0 \in [0,1]$ and $\beta \in \mathbb{R}^+$ are user-predefined parameters. While β determines the relative importance of the heuristic information, r_0 balances between exploitation and exploration: if $r \le r_0$, the algorithm favors the solution component with the best compromise between pheromone and heuristic value, whereas if $r > r_0$ the algorithm explores the space of solutions by choosing a solution component $c_i^j \in \mathscr{C}_i$ according to an empirical distribution whose probability mass function is defined by $f_Q(q) = Pr(Q = q) = Pr\{c_i^j \in \mathscr{C}_i : Q(c_i^j) = q\} = p(c_i^j)$, where

$$p(c_i^j) = \frac{\tau_i^j [\eta(c_i^j)]^\beta}{\sum_{c_i^k \in \mathscr{C}_i} \tau_i^k [\eta(c_i^k)]^\beta}. \tag{17}$$

3) Local Update: The modifications on $\varphi_v, v \in \mathcal{V}$ caused by the local pheromone update process only have impact on the trail followed by the ant in progress (see lines 6 and 13 in Procedure 3). The main objective of this rule is to bias the ant toward nodes it has already visited during the construction of the solution with the aim of aggregating regenerators across the network. After selecting each solution component c_i^j, all the nodes contained in s_j update their pheromone values τ_i^j. The updating rule is defined as follows:

$$\varphi_v(t+1) = \varphi_v(t) + \alpha e^{-\psi \Delta_r}, \quad \forall v \in s_j, \tag{18}$$

where $\alpha, \psi \in \mathbb{R}^+$ are two more user-specified parameters and $\Delta_r = |s_j| - 1$. Note that when the option selected s_j only contains one regeneration node $\Delta_r = 0$, thereby maximizing the quantity of pheromone deposited by the ant. Moreover, ψ is a decay constant which also controls the amount of deposition.

4) Global Update: After a group of *MaxAnts* have constructed their respective solutions (stored in Ω_{IT}), a global updating rule is applied to all solution components contained in each $\mathscr{R}_x \in \Omega_{IT}$. The aim of this rule is to guide the next group of ants toward high quality solution components. To this end, node pheromone values are updated as follows:

$$\varphi_v(t+1) = (1-\vartheta)\varphi(t) + \vartheta e^{-\phi(g(\mathscr{R}_x) - g(\mathscr{R}_{BEST}))}, \quad \forall v \in s_j : \Omega_x \ni s_j, \forall \Omega_x \in \Omega_{IT}, \tag{19}$$

where $\vartheta, \phi \in \mathbb{R}^+$ are two user-predefined parameters. Note that ϑ controls the speed at which pheromone evaporates and ϕ is another decay factor. Finally, the exponential factor favors the deposit of pheromone on those regeneration nodes belonging to the best solutions obtained by each group of ants. All the parameters required to define the ACO RPD heuristic here presented will be adjusted in Section VII.

The worst case complexity of this algorithm is given by

$$O(GlobItr \cdot MaxAnts \cdot |\mathscr{P}^o| \cdot \Theta), \tag{20}$$

where the first three factors represent the *repeat-until* and *for all* loops, and Θ in this case represents the maximum number of solution components that an ant may need to evaluate before applying the state transition rule.

D. BRKGA Algorithm

BRKGA is a type of genetic algorithm (GA) which has recently been proposed to effectively solve complex optimization problems, for instance, network related problems such as routing in IP networks and RWA in optical networks [33,34]. In most cases, this meta-heuristic is characterized by being able to obtain high quality solutions in very short times. In BRKGA, each individual is an array of n_g genes called a *chromosome*. In addition, each gene is assigned a value, called an *allele*, in the real interval [0,1]. Each chromosome encodes a solution of the problem and a *fitness* level (i.e., the objective function value $g(\cdot)$). Like any other GA algorithm, BRKGA evolves a set of p individuals, called a *population*, over a number of generations until a stopping criterion is met

Procedure 3 Ant Colony Optimization (ACO)

INPUT: $\mathscr{P}^o, \mathscr{S}_p \ \forall p \in \mathscr{P}^o, GlobItr, MaxAnts$
OUTPUT: $g(\mathscr{R}_{BEST})$

```
1: InitializePheromoneValues(𝒯)
2: ℛ_BEST ← ∅, count ← 0
3: repeat
4:   Ω_IT ← ∅, ant ← 0
5:   repeat
6:     Local Pheromones 𝒯_LOC ← 𝒯
7:     Ω_x ← ∅
8:     Λ ← random order of paths in 𝒫^o
9:     for all path p ∈ Λ do
10:      c_p^x ← getNextSolutionComponent(𝒯_LOC)
11:      Take s_x from c_p^x
12:      Ω_x ← Ω_x ∪ {s_x}
13:      UpdateLocalPheromones(c_p^x, 𝒯_LOC)
14:    end for
15:    Generate ℛ_x from Ω_x
16:    if g(ℛ_x) < g(ℛ_BEST) then
17:      ℛ_BEST ← ℛ_x
18:    end if
19:    Ω_IT ← Ω_IT ∪ {Ω_x}
20:    ant ← ant + 1
21:  until ant ≥ MaxAnts
22:  UpdateGlobalPheromones(Ω_IT, 𝒯)
23:  count ← count + 1
24: until count ≥ GlobItr
```

(e.g., number of iterations, generations without improvement). The subsequent generations consist of individuals which are created by means of (1) a mating process (two chromosomes of the current population are combined), (2) a set of high quality chromosomes of the current generation (called elite set p_e), which are copied unchanged, and (3) a set of new randomly generated chromosomes (called mutants) p_m, which should help the algorithm escape from local optima.

To produce offspring through the mating process, two chromosomes of the current population (one elite and another non-elite) are selected at random and then combined. The offspring can inherit alleles from both parents (though with a bias defined by the probability of inheriting from the elite parent ρ_e). In order to compute the fitness of each chromosome, a deterministic algorithm, called a *decoder*, is used. The decoder is the only problem-dependent part of the BRKGA algorithm, and, hence, is the only part that needs to be specifically developed to solve the RPD problem.

The pseudo-code of our decoder algorithm is shown in Procedure 4. In this case, each chromosome contains $n_g = |\mathscr{N}|$ genes (i.e., one per node in the network), and the metric value for each node corresponds to the value of the allele (i.e., the value of the gene). We select the option $s \in \mathscr{S}_p$ which minimizes the cost in terms of that metric. This cost corresponds to the sum of the alleles for all the nodes in a regeneration option (denoted by $c(s)$ in Procedure 4).

Considering a population size $p = n_g = |\mathscr{N}|$ and a maximum number of generations MG, the complexity of the BRKGA is given by

$$O(MG \cdot |\mathscr{N}| \cdot Proc.4). \tag{21}$$

Procedure 4 BRKGA Decoder Algorithm

INPUT: $\mathscr{N}, chromo, \mathscr{P}^o, \mathscr{S}_p \ \forall p \in \mathscr{P}^o$
OUTPUT: $fitness$

```
1: for all node n ∈ 𝒩 do
2:   n.metric ← chromo.getGene(n)
3: end for
4: ℛ_x ← ∅
5: for all path p ∈ 𝒫^o do
6:   for all option s ∈ 𝒮_p do
7:     for all node n ∈ s do
8:       c(s) ← c(s) + n.metric
9:     end for
10:  end for
11:  Select s ∈ 𝒮_p with minimum c(s) and generate z_p
12:  ℛ_x ← ℛ_x ∪ {z_p}
13: end for
14: fitness ← g(ℛ_x)
```

The complexity of the decoder algorithm in Procedure 4 is obtained as follows:

$$Proc.4 = O(|\mathscr{P}^o| \cdot \Theta \cdot (\delta - 2)), \tag{22}$$

where each term represents, respectively, $|\mathscr{P}^o|$ the most outer loop (line 5), the maximum number of regeneration options (loop in line 6) and the largest path $p \in \mathscr{P}^o$ having all its intermediate nodes as regeneration sites (loop in line 7).

E. Regenerator Dimensioning

Given the set of valid paths $p \in \mathscr{P}^o$, in this step, a solution for the RP $\mathscr{R} = \bigcup_{p \in \mathscr{P}^o} \mathbf{z}_p$ and the number of regenerators to be installed in the nodes is determined.

Let ρ_v^o denote the offered traffic load requiring regeneration at node v. To estimate ρ_v^o (approximately) we add up the traffic load ρ_p offered to each path $p \in \mathscr{P}^o$ that both crosses and undergoes regeneration at node v:

$$\rho_v^o = \sum_{p \in \mathscr{P}^o : \mathscr{V}_p \ni v} \ \sum_{s \in \mathscr{S}_p : s \ni v} z_{ps} \rho_p. \tag{23}$$

Similarly,

$$\rho_v = \sum_{p \in \mathscr{P}^o : \mathscr{V}_p \ni v} \rho_p \tag{24}$$

denotes an estimation of the maximal traffic load that is subject to regeneration at node $v \in \mathscr{V}$.

Eventually, we define a regenerator pool dimensioning function $F_v(\cdot) : (R^+, R^+) \mapsto \mathbb{Z}^+$, which for a given traffic load ρ_v^o determines the minimum number of regenerators to be allocated in node v. This number must ensure that a given target burst blocking probability (B^{QoT}) for bursts competing for regeneration resources is met. Assuming Poisson arrivals and fairness in the access to regenerator pools among bursts, such a function is given by the following discontinuous, step-increasing function:

$$F_v(\rho_v^o) = \left\lceil B^{-1}(\rho_v^o, B^{\mathrm{QoT}}) \right\rceil, \tag{25}$$

where $B^{-1}(\rho_v^o, B^{\text{QoT}})$ is the inverse function of the erlang B loss formula, which for a given number of regenerators $r \in \mathbb{N}$ available at node v can be calculated as

$$B(\rho_v^o, r) = \frac{(\rho_v^o)^r / r!}{\sum_{k=0}^{r} (\rho_v^o)^k / k!}. \tag{26}$$

It is worth noticing that the Poisson arrivals which lead to an erlang B formula for the dimensioning of regenerator pools can be replaced with another distribution for which the blocking probability is attainable.

For the purpose of computation, it is convenient to define a_r as the maximal load supported by r regenerators given a B^{QoT}, i.e., $a_r = B^{-1}(r, B^{\text{QoT}})$. Although there is no close formula to compute the inverse of Eq. (26), we can make use of a line search method to find the root ρ^* of the function $f(\rho) = B^{\text{QoT}} - B(\rho, r)$ so that the value of a_r is approximated by $a_r = \rho^*$ for any index r. As a result, the regenerator dimensioning algorithm, which we apply to find the number of regenerators in a pool, is presented in Procedure 5.

Procedure 5 Regenerator Pool Dimensioning

INPUT: $\mathscr{R}, \mathscr{P}^o$
OUTPUT: F_v

```
for all nodes v ∈ V do
    Compute ρ_v^o according to R
    r ← 0
    while ρ_v^o > a_r do
        r ← r + 1
    end while
    F_v ← r
end for
```

Let R denote the number of regenerators required in the most loaded node, that is, $R = \max\{F_v(\rho_v) : v \in \mathcal{V}\}$, then Procedure 5 is a polynomial time algorithm of complexity $O(R)$. We point out that a vector $\mathbf{a} = (a_1, \ldots, a_R)$, which determines the number of regenerators required for all cases between 1 and R, can be precomputed once at the very beginning of the RPD algorithm.

VII. Results and Discussion

In this section, we first present the details of the simulation scenario considered. Then, we use CPLEX [35] to obtain the results of the optimal MILP formulation (MP1) [12] and compare its results with those of all the RPD methods proposed in Section VI as well as with those of the load-based MILP heuristic (MP2/3) also proposed in [12]. Finally, we study the performance of the T-OBS network architecture under selected RPD methods in order to prove that they are effective at keeping OSNR losses under control.

A. Network Scenario and Parameter Tuning

The evaluation has been performed by considering five different network topologies (see details in Appendix A). In this work, we consider 19 dB as the $T_{\text{osnr-min}}$ threshold, a value which is commonly used for the experimental assessment of translucent optical networks with such network links [21]. Moreover, we introduce an additional 2 dB OSNR penalty ($T_{\text{osnr-pen}}$) so as to account for the signal degradation caused by non-linear impairments. Hence, we set T_{osnr} to 21 dB in all our experiments. Note that T_{osnr} also determines the number of paths that require regeneration (i.e., $|\mathscr{P}_o|$), and, hence, the level of complexity that is given to the problem. $|\mathscr{P}_o|$ values are reported in Table II.

TABLE II
$\mathscr{P}^o$ Size Values

Network	USA–Can	German	Core	Basic	Large
$\lvert\mathscr{P}_o\rvert$	657	752	55	462	919

TABLE III
BRKGA Parameter Values

p	n_g	MG	ρ_e	p_e	p_m
$\lvert\mathscr{N}\rvert$	$\lvert\mathscr{N}\rvert$	100	0.7	0.2	0.2

It must be pointed out that, as shown in Eq. (11), the size of set $\mathscr{S}_p, p \in \mathscr{P}^o$ is exponential to the size of the input. Hence, depending on the network instance (see topology details in Appendix A), this fact may lead to heuristic algorithms requiring very high, and thus impractical, computational times. In view of this, our strategy is to consider a maximum of $K = 25$ options to fill $\mathscr{S}_p$, that is, $\mathscr{S}_p = \{s_1, \ldots, s_K\}$. To be precise, the 25 smallest regeneration options, ordered according to their size $|s_j|, j = 1 \ldots |\mathscr{S}_p|$, are considered. Since all the RPD methods rely on random parameters to generate their respective solutions (e.g., the randomly built initial solution $\mathscr{R}_o$ in KLS), we conduct a set of independent runs for each method and take as the result the best value found. However, both the ACO and BRKGA meta-heuristics require some additional parameter tuning. After performing some preliminary experiments, we set the parameters of the BRKGA meta-heuristic to the values summarized in Table III. Due to both the facts that ACO requires the tuning of a rather large set of parameters and that these may require a different setup in each network topology, we perform a large set of experiments considering a number of different values for each parameter. The constant parameters σ and k are set to 0.1 and 1, respectively. Besides, we observe that the best solutions are always obtained when values of r_0 close to 1 are considered. Thus, we fix r_0 to 0.9. To obtain the rest of the parameter values, we run the ACO algorithm with $GlobItr$ = 500, $MaxAnts$ = 100, loads of 15 and 20.8 erlangs and the values proposed in Table IV, thus conducting 450 experiments per network topology. Note that we assume that both decay factors have the same value. We observe that the results do not report any significant dependence on the network load scenario considered. The parameter values selected are shown in Table V.

B. Resolution Methods Comparison

First, in Table VI, we provide the number of regenerators as well as the optimality gaps found by CPLEX when solving

TABLE IV
ACO PARAMETER VALUES EVALUATED

$\psi = \phi$	0.25, 0.75, 1.75
ϑ	0.001, 0.01, 0.1
β	0.5, 1, 2, 3, 4
α	0, 0.001, 0.005, 0.01, 0.1

TABLE V
ACO PARAMETERS SELECTED FOR EACH NETWORK TOPOLOGY

Network	$\psi = \phi$	ϑ	β	α
USA–Can	0.75	0.1	4	0.1
German	0.25	0.001	4	0.01
Core	0.25	0.001	4	0.005
Basic	0.25	0.01	4	0.01
Large	0.25	0.001	4	0.005

MP1 with the time limit set to 1 h. In addition, we include the number of regenerators required when an opaque network scenario is considered. In this experiment, we assume a target $B^{\mathrm{QoT}} = 10^{-3}$, and loads equal to 20.8 and 15 erlangs. One can observe that in both the Core and Basic networks (i.e., the smallest problem instances) CPLEX is able to obtain results equal or very close to optimality, whereas in the larger networks gaps of up to 25.6% are reported. Second, in Table VII, we report the results (amount of regenerators to be deployed) of all the RPD heuristics presented (MP2/3 included) in the same network scenario. In addition, Table VIII reports the average computational times required by each of the methods when the load is set to 20.8 erlangs. Whilst in the Core network all methods perform quite similarly, in all the other topologies both the BRKGA and MP2/3 stand out as the best methods. However, BRKGA always provides the best solution to the problem and it is only slightly outperformed by MP1 in the Basic instance. Furthermore, it reaches its solutions within very short running times compared to all the other methods evaluated. Hence, BRKGA stands out as a very powerful algorithm providing a high quality trade-off between optimality and complexity. To further study these algorithms, in Fig. 4, we show the results of all the heuristics in some of the considered networks and for some exemplary B^{QoT} target values. Again, it is possible to see that BRKGA always obtains the best results, though it is closely followed by MP2/3 in all the networks, except for the USA–Can topology, where MP2/3 exhibits a very poor performance and it is even outperformed by ACO. In the next subsection, we evaluate the performance of some of these heuristic methods when applied to the T-OBS network architecture proposed.

C. Impact on the T-OBS Network Performance

The RPD heuristics proposed in this paper must ensure that burst losses due to unacceptable OSNR levels are kept under control, and, thus, that the predefined target loss rate B^{QoT} is met. In order to verify that this is accomplished, we conduct a set of simulations over both the German and Large network topologies. Aiming at providing illustrative plots of the scenario in hand, we consider the best and worst RPD heuristic for each network, that is, the BRKGA as the best method in both cases, and the KLS (German) and RG (Large). In addition, we include the transparent and opaque scenarios and use them as benchmark references. In both experiments we consider B^{QoT} values equal to 10^{-3} and 10^{-5}. The results obtained are presented in Fig. 5 for the German network and in Fig. 6 for the Large network. One can note that with the progressive and even placement of regenerators (i.e., regenerators are fairly distributed among all regenerator sites) the burst loss probability (BLP) moves toward either the target performance B^{QoT} or the opaque performance. In both Fig. 5 and Fig. 6, once all the regenerators are deployed, we can observe two different situations: if B^{QoT} is set to 10^{-3}, OSNR losses are still predominant due to the low contention losses of this scenario; if B^{QoT} is set to 10^{-5}, in contrast, contention losses become predominant in the network. Note that in both figures provided, the BLP found in the case where contention losses are predominant slightly improves that of the opaque case. This is due to the differences in node architectures between the opaque and translucent networks: whilst the opaque network relies on in-line regenerators as in [7], our translucent architecture operates in the feed-back mode as proposed in [8], and, hence, bursts remain in the electrical buffer until a free wavelength is found at the desired output link. Finally, and due to the fact that we are

TABLE VI
MP1 RESULTS AND OPTIMALITY GAPS OBTAINED BY CPLEX

Method	USA–Can	German	Core	Basic	Large
Load = 20.8					
MP1	634	606	146	752	1231
Gap (%)	9.4	22.7	0	0.7	2.7
Load = 15					
MP1	482	486	115	581	981
Gap (%)	7.9	25.6	0	0.5	7.2
Opaque	3904	5632	1472	2624	3648

TABLE VII
RPD ALGORITHMS RESULTS EVALUATION

Method	USA–Can	German	Core	Basic	Large
Load = 20.8					
MP2/3	654	518	147	761	1241
BRKGA	607	511	146	756	1223
ACO	636	538	147	769	1271
KLS	708	659	148	803	1296
RG	727	585	148	870	1378
Load = 15					
MP2/3	498	404	116	586	951
BRKGA	465	397	115	582	940
ACO	502	426	116	595	972
KLS	563	536	116	638	1028
RG	570	467	117	678	1076

TABLE VIII
RPD ALGORITHMS EXECUTION TIME (SECONDS)

Method	USA–Can	German	Core	Basic	Large
MP2/3	43	116	1	19	59
BRKGA	10	19	1	3	10
ACO	117	174	6	33	142
KLS	37	103	1	15	64
RG	1	2	0.5	1	1.8

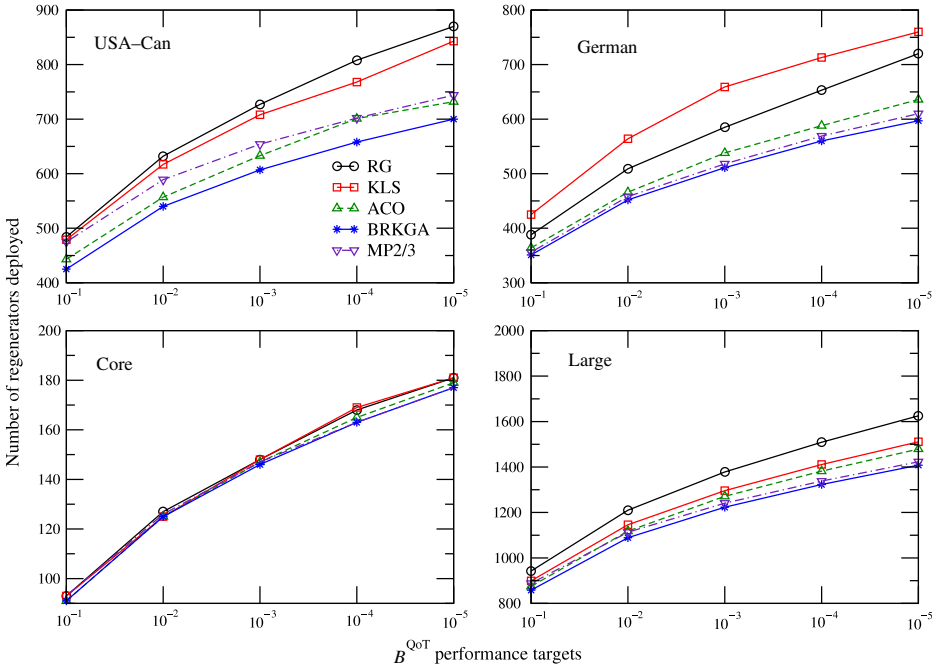

Fig. 4. (Color online) RPD algorithms performance in the USA–Can, German, Core and Large networks under different B^{QoT} targets.

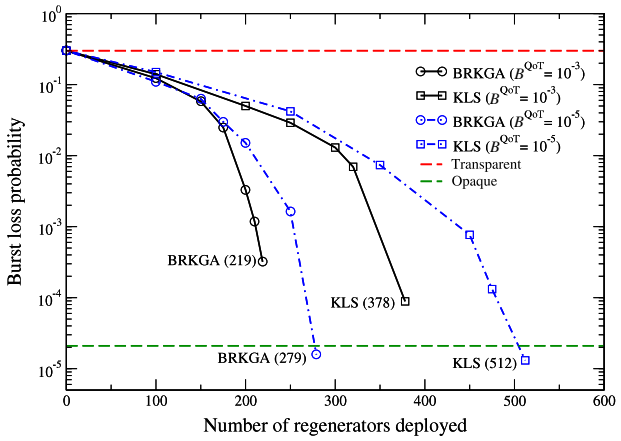

Fig. 5. (Color online) BRKGA versus KLS performance comparison in the German network.

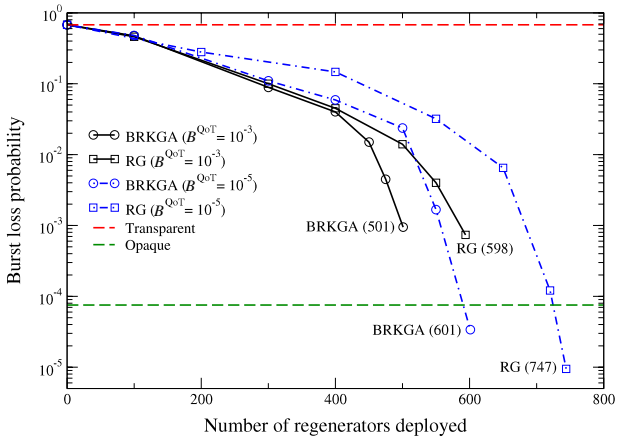

Fig. 6. (Color online) BRKGA versus RG performance comparison in the Large network.

addressing an offline planning/dimensioning of the network, in this last experiment, we evaluate the impact that load variations have on both losses due to contention in network links and losses resulting from unacceptable OSNR levels. To this end, we dimension the T-OBS network considering the Large topology, a load of 9 erlangs and a target $B^{QoT} = 10^{-3}$. In this scenario, BRKGA provides a solution requiring 633 regenerators to be deployed. Table IX reports the share of burst losses for different load values. Although we can observe that for higher loads the percentage of OSNR-based losses inevitably increases, we assume that the dimensioning of the network is made according to a worst case scenario. Therefore, it can be concluded that our approach guarantees that OSNR losses are kept well below those caused by burst contentions in network links.

VIII. Conclusions and Future Work

In this paper, we have proposed several methods to solve the RRPD problem in a translucent OBS network. To this end, we have focused on the problem of PLIs in OBS networks. In particular, we have presented a T-OBS network architecture consisting of all-optical TAS nodes equipped with a limited number of O/E/O regenerators. Then, we have provided an OSNR model to evaluate the impact of the main PLIs (i.e., ASE noise and splitting losses) and illustrated a method to compute

TABLE IX
SHARE OF BURST LOSSES FOR A BRKGA DIMENSIONING IN THE LARGE NETWORK

Load	7	7.5	8	8.5	9	9.5	10
Contention (%)	93.7	90	88.5	84.6	80.1	73	67.1
OSNR (%)	6.3	10	11.5	15.4	19.9	27	32.9

a power budget and noise analysis between two TAS OBS core nodes. Afterward, this model has been used to address the RRPD problem. To be precise, we have decomposed RRPD into the routing problem and the RPD problem and eventually solved the resulting R+RPD problem. We have presented an unsplittable routing strategy which is based on an MILP formulation aimed at reducing congestion in bottleneck network links. The routing solution obtained has then been used as input for the RPD problem. To solve RPD, we have proposed several heuristic methods which are aimed at minimizing the number of regenerators required to meet a predefined target loss performance due to the impact of PLIs. We have thoroughly evaluated and compared these methods against both an optimal and a heuristic MILP formulation of the RPD problem. The results have shown that BRKGA is, among all the methods evaluated, the one providing the best trade-off between optimality and complexity. Finally, we have conducted a series of exhaustive simulations in the T-OBS network and concluded that both the architecture and RPD models proposed in this paper ensure that, according to a pre-specified target QoT performance, losses caused by OSNR signal degradation are kept satisfactorily under control and do not impact negatively the overall T-OBS network performance. In our future work, we plan to extend our model to consider the case of an online/dynamic scenario.

APPENDIX A: SIMULATION SCENARIO

In our simulation scenario, we consider several topologies (see Fig. 7): a set of pan-European [36] networks known as Large (a), Basic (b) and Core (c) with 37, 28 and 16 nodes and 57, 41 and 23 links, respectively; the JANOS-US-CA [37] (d), a reference network that interconnects cities in the USA and Canada with 39 nodes and 61 links and a German backbone topology known as GERMAN50 [37] (e), with 50 nodes and 88 links. In addition, Table X summarizes, for all the networks, some interesting parameters regarding both the number of nodes (e.g., network diameter) and the distance of their respective optical end-to-end paths.

Network links are bidirectional and dimensioned with the same number of wavelengths $M = 32$. The transmission bitrate is set to 10 Gbps.

We assume that each node is both an edge and a core bufferless node capable of generating bursts destined for any other nodes. We consider the offset time emulated OBS network architecture (E-OBS) [38] and the just-in-time (JIT) [39] resources reservation protocol. For the sake of simplicity, the switching and processing times are neglected.

The traffic is uniformly distributed between nodes. We assume that each edge node offers the same amount of traffic to the network; this offered traffic is normalized to the transmission bitrate and expressed in erlangs. In our context, an erlang corresponds to the amount of traffic that occupies an entire wavelength (e.g., 20 erlangs mean that each edge node generates 200 Gbps).

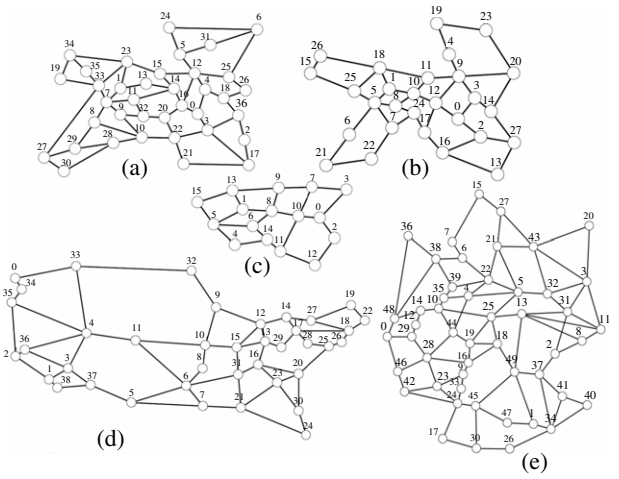

Fig. 7. The topologies considered: (a) Large (37 nodes), (b) Basic (28 nodes), (c) Core (16 nodes), (d) USA–Can (39 nodes), (e) German (50 nodes).

TABLE X
PATH CHARACTERISTICS: NUMBER OF NODES TRAVERSED AND DISTANCE (km)

Network	Max. nodes	Avg. nodes	Max. length	Avg. length
USA–Can	12	5.36	3297	1360.55
German	13	5.5	1037.6	421.1
Core	7	3.7	2912	1238.4
Basic	10	4.75	6505	2094.4
Large	12	5.1	7824	2410.1

Bursts are generated according to a Poisson arrival process and have exponentially distributed lengths. The mean duration of a burst ($1/\mu$) is 100 μs (1 Mb). Note that due to both the Poisson assumption and the fact that we neglect both the switching and processing times of bursts, the burst size does not have any impact on the results obtained [40]. In obtaining the simulation results, we have estimated 99% confidence intervals. However, since the confidence intervals found are very narrow, we do not plot them in order to improve readability.

All simulations have been conducted on the JAVOBS [41] network simulator on an Intel Core 2 Quad 2.67 GHz with 4 GB RAM. We use CPLEX (version 12.1) [35] as the underlying MILP-solver for the Eqs. (RMILP1), (RMILP2), MP1 and MP2/3 problems.

ACKNOWLEDGMENTS

The work described in this paper was carried out with the support of the STRONGEST project, an Integrated Project funded by the European Commission through the 7th ICT-Framework Programme; the Spanish Ministry of Science and Innovation under the "DOMINO" project (Ref. TEC2010-18522); the Catalan Government under the contract SGR-1140; and the Polish Ministry of Science and Higher Education.

REFERENCES

[1] B. Ramamurthy, H. Fenq, D. Datta, J. P. Heritage, and B. Mukherjee, "Transparent vs. opaque vs. translucent wavelength-routed optical networks," in *Proc. IEEE/OSA OFC'1999*, San Diego, CA, Feb. 1999, vol. 1, pp. 59–61.

[2] R. Martínez, C. Pinart, F. Cugini, N. Andriolli, L. Valcarenghi, P. Castoldi, L. Wosinska, J. Comellas, and G. Junyent, "Challenges and requirements for introducing impairment-awareness into the management and control planes of ASON/GMPLS WDM networks," *IEEE Commun. Mag.*, vol. 44, no. 12, pp. 76–85, Dec. 2006.

[3] G. Shen and R. S. Tucker, "Translucent optical networks: the way forward," *IEEE Commun. Mag.*, vol. 45, no. 2, pp. 48–54, Feb. 2007.

[4] Y. Lee, G. Bernstein, D. Li, and G. Martinelli, "A framework for the control of wavelength switched optical networks (WSON) with impairments," *IETF Internet draft*, Oct. 2010.

[5] R. Muñoz, R. Martínez, and R. Casellas, "Challenges for GMPLS lightpath provisioning in transparent optical networks: wavelength constraints in routing and signalling," *IEEE Commun. Mag.*, vol. 47, no. 8, pp. 26–34, Aug. 2009.

[6] C. Qiao and M. Yoo, "Optical burst switching (OBS)–A new paradigm for an optical Internet," *J. High Speed Netw.*, vol. 8, no. 1, pp. 69–84, Jan. 1999.

[7] H. Buchta and E. Patzak, "Analysis of the physical impairments on maximum size and throughput of SOA-based optical burst switching nodes," *J. Lightwave Technol.*, vol. 26, no. 16, pp. 2821–2830, Aug. 2008.

[8] O. Pedrola, D. Careglio, M. Klinkowski, and J. Solé-Pareta, "Modelling and performance evaluation of a translucent OBS network architecture," in *Proc. IEEE Globecom 2010*, Miami, FL, Dec. 2010, pp. 1–6.

[9] X. Yang and B. Ramamurthy, "Sparse regeneration in translucent wavelength-routed optical networks: Architecture, network design and wavelength routing," *Photonic Network Commun.*, vol. 10, no. 1, pp. 39–53, Jan. 2005.

[10] S. Pachnique, T. Paschenda, and P. M. Krummrich, "Physical impairment based regenerator placement and routing in translucent optical networks," in *Proc. IEEE/OSA OFC/NFOEC 2008*, San Diego, CA, Feb. 2008, pp. 1–3.

[11] W. Zhang, J. Tang, K. E. Nygard, and C. Wang, "REPARE: Regenerator placement and routing establishment in translucent networks," in *Proc. IEEE Globecom 2009*, Nov. 2009, pp. 1–7.

[12] O. Pedrola, D. Careglio, M. Klinkowski, and J. Solé-Pareta, "RRPD strategies for a T-OBS network architecture," in *Proc. IEEE HPSR 2011*, Cartagena, Spain, July 2011, pp. 95–100.

[13] M. Dorigo and T. Stützle, *Ant Colony Optimization*. The MIT Press, Cambridge, MA, 2004.

[14] J. Gonçalves and M. Resende, "Biased random-key genetic algorithms for combinatorial optimization," *J. Heuristics* (posted 27 August 2010, in press).

[15] A. Sen, S. Murthy, and S. Bandyopadhyay, "On sparse placement of regenerator nodes in translucent optical networks," in *Proc. IEEE Globecom 2008*, Nov. 2008, pp. 1–6.

[16] S. Azodolmolky, M. Klinkowski, E. Marin, D. Careglio, J. Solé-Pareta, and I. Tomkos, "A survey on physical layer impairments aware routing and wavelength assignment algorithms in optical networks," *Comput. Netw.*, vol. 53, no. 7, pp. 926–944, May 2009.

[17] K. Manousakis, P. Kokkinos, K. Christodoulopoulos, and E. Varvarigos, "Joint online routing, wavelength assignment and regenerator allocation in translucent optical networks," *J. Lightwave Technol.*, vol. 28, no. 8, pp. 1152–1163, Apr. 2010.

[18] Y. Fan and B. Wang, "Physical impairment aware scheduling in optical burst switched networks," *Photonic Network Commun.*, vol. 18, no. 2, pp. 244–254, Oct. 2009.

[19] B. G. Bathula, R. R. C. Bikram, V. M. Vokkarane, and S. Talabattula, "Quality of transmission aware manycasting over optical burst-switched (OBS) networks," *J. Opt. Commun. Netw.*, vol. 2, no. 10, pp. 820–829, Oct. 2010.

[20] H. Buchta, C. M. Gauger, and E. Patzak, "Maximum size and throughput of SOA-based optical burst switching nodes with limited tuning-range wavelength converters and FDL buffers," *J. Lightwave Technol.*, vol. 26, no. 16, pp. 2919–2927, Aug. 2008.

[21] R. Martínez, R. Casellas, R. Muñoz, and T. Tsuritani, "Experimental translucent-oriented routing for dynamic lightpath provisioning in GMPLS-enabled wavelength switched optical networks," *J. Lightwave Technol.*, vol. 28, no. 8, pp. 1241–1255, Apr. 2010.

[22] H. Pereira, D. A. R. Chaves, C. J. A. Bastos-Filho, and J. F. Martins-Filho, "OSNR model to consider physical layer impairments in transparent optical networks," *Photonic Network Commun.*, vol. 18, no. 2, pp. 137–149, Oct. 2009.

[23] T. Tsuritani, M. Miyazawa, S. Kashihara, and T. Otani, "Optical path computation element interworking with network management system for transparent mesh networks," in *Proc. IEEE/OSA OFC/NFOEC 2008*, San Diego, CA, Feb. 2008, pp. 1–10.

[24] INPHENIX [Online]. Available: http://www.inphenix.com/soa_devices.html.

[25] MRV [Online]. Available: http://www.mrv.com/product/MRV-LD-OAB.

[26] M. Mestre, J. M. Fabrega, J. A. Lazaro, V. Polo, A. Djupsjobacka, M. Forzati, P. J. Rigole, and J. Prat, "Tuning characteristics and switching speed of a modulated grating Y structure laser for wavelength routed PONs," in *Proc. ANIC 2010*, Karlsrhue, Germany, June 2010, pp. 1–2.

[27] M. Klinkowski, J. Pedro, D. Careglio, M. Pióro, J. Pires, P. Monteiro, and J. Solé-Pareta, "An overview of routing methods in optical burst switching networks," *Opt. Switching Netw.*, vol. 7, no. 2, pp. 41–53, Apr. 2010.

[28] J. Kleinberg and E. Tardos, *Algorithm Design*. Addison-Wesley, 2005, pp. 661–706.

[29] M. Dorigo and C. Blum, "Ant colony optimization theory: A survey," *Theor. Comput. Sci.*, vol. 344, no. 2–3, pp. 243–278, 2005.

[30] R. Garlick and R. Barr, "Dynamic wavelength routing in WDM networks via ant colony optimization," *Lect. Notes Comput. Sci.*, vol. 2463, pp. 27–41, 2002.

[31] S. Ngo, X. Jiang, and S. Horiguchi, "An ant-based approach for dynamic RWA in optical WDM networks," *Photonic Network Commun.*, vol. 11, no. 1, pp. 39–48, 2006.

[32] J. Triay and C. Cervelló-Pastor, "An ant-based algorithm for distributed routing and wavelength assignment in dynamic optical networks," *J. Sel. Areas Commun.*, vol. 28, no. 4, pp. 542–552, May 2010.

[33] T. Noronha, M. Resende, and C. Ribeiro, "A biased random-key genetic algorithm for routing and wavelength assignment," *J. Global. Optim.*, vol. 50, no. 3, pp. 503–518, 2011.

[34] R. Reis, M. Ritt, L. Buriol, and M. Resende, "A biased random-key genetic algorithm for OSPF and DEFT routing to minimize network congestion," *Int. Trans. Oper. Res.*, vol. 18, no. 3, pp. 401–423, May 2011.

[35] IBM ILOG CPLEX [Online]. Available: http://www-01.ibm.com/software/integration/optimization/cplex/.

[36] S. De Maesschalck, D. Colle, I. Lievens, M. Pickavet, P. Demeester, C. Mauz, M. Jaeger, R. Inkret, B. Mikac, and J. Derkacz, "Pan-European optical transport networks: An availability-based comparison," *Photonic Network Commun.*, vol. 5, no. 3, pp. 203–225, May 2003.

[37] S. Orlowski, M. Pióro, A. Tomaszewski, and R. Wessäly, "SNDlib 1.0 survivable network design library," *Networks*, vol. 55, no. 3, pp. 276–286, May 2010.

[38] M. Klinkowski, D. Careglio, J. Solé-Pareta, and M. Marciniak, "Performance overview of the offset time emulated OBS network architecture," *J. Lightwave Technol.*, vol. 27, no. 14, pp. 2751–2764, July 2009.

[39] J. Y. Wei and R. I. McFarland, "Just-in-time signaling for WDM optical burst switching networks," *J. Lightwave Technol.*, vol. 18, no. 12, pp. 2019–2037, Dec. 2000.

[40] Z. Rosberg, H. L. Vu, M. Zukerman, and J. White, "Performance analyses of optical burst-switching networks," *IEEE J. Sel. Areas Commun.*, vol. 21, no. 7, pp. 1187–1197, Sept. 2003.

[41] O. Pedrola, S. Rumley, M. Klinkowski, D. Careglio, C. Gaumier, and J. Solé-Pareta, "JAVOBS: a flexible simulator for OBS network architectures," *J. Netw.*, vol. 5, no. 2, pp. 256–264, Feb. 2010.